Science Advances

AAAS

advances.sciencemag.org/cgi/content/full/2/10/e1601026/DC1

Supplementary Materials for

Tunable and label-free virus enrichment for ultrasensitive virus detection using carbon nanotube arrays

Yin-Ting Yeh, Yi Tang, Aswathy Sebastian, Archi Dasgupta, Nestor Perea-Lopez, Istvan Albert, Huaguang Lu, Mauricio Terrones, Si-Yang Zheng

Published 7 October 2016, *Sci. Adv.* **2**, e1601026 (2016)
DOI: 10.1126/sciadv.1601026

The PDF file includes:

- fig. S1. Fabrication process and the testing setup of the CNT-STEM.
- fig. S2. AACVD for N-MWCNT synthesis.
- fig. S3. Raman spectra of the newly synthesized N-MWCNT structures on silicon substrates and the effect of the synthesis time on the height, diameter, and density of the aligned N-MWCNT structure.
- fig. S4. Characterization of size-based particle capture by CNT-STEM.
- fig. S5. Laser diffraction measurement of the size distribution of the LP AIV H5N2 strain used in this study.
- fig. S6. Standard curve for the rRT-PCR detection of H5N2 AIV (n = 4 each).
- fig. S7. Capture efficiency measurement of CNT-STEM with 25-, 95-, and 325-nm intertubular distances when loading H5N2 AIV of 10^6 EID_{50}/ml of titer into each device (n = 6).
- fig. S8. rRT-PCR curves of H5N2 AIV samples of 10 and 10^2 EID_{50}/ml of titers without enrichment and those of 0.1 and 1 EID_{50}/ml of titers with CNT-STEM enrichment (n = 6).
- fig. S9. The compatibility test of N-MWCNT to rRT-PCR.
- fig. S10. Diagram of data processing pipeline for NGS.
- fig. S11. SEM images of CNT-STEM after processing field sample containing AIV.
- fig. S12. rRT-PCR detection of the H11N9 AIV duck swab with and without CNT-STEM enrichment.
- fig. S13. Structural mechanics analysis of N-MWCNT forest.
- fig. S14. Analysis device yield, reliability, and failure modes.

- fig. S15. Fluorescent image of FITC-conjugated IgG pass through CNT-STEM of 25-nm in interturbular distance.
- fig. S16. Calculated distance between the iron particles based on the Delaunay triangle selection algorithm.
- table S1. Measurement of the intertubular distance of N-MWCNT forest and the corresponding critical particle sizes of CNT-STEM.
- table S2. Assembled contigs of the LP H5N2 AIV sample enriched by CNT-STEM.
- table S3. Phylogenetic analysis of the sequenced H5N2 strain (A/chicken/PA/7659/1985) to closely related H5N2 AIV strains isolated from United States/Canada in GenBank.
- table S4. Assembled contigs of the H11N9 AIV field sample enriched by CNT-STEM.
- table S5. Phylogenetic analysis of the emerging H11N9 strain (A/duck/PA/02099/2012) to previously reported and closely related AIV strains.
- table S6. Comparison of contigs of the unknown virus (IBDV/turkey/PA/00924/14) generated by de novo assembly after CNT-STEM enrichment and NGS to the closest IBDV strains in GenBank.
- table S7. Single-nucleotide polymorphism/variant analysis of the "unknown" virus (IBDV/turkey/PA/00924/14) to sequenced IBDV virus strains.
- table S8. Comparison of CNT-STEM to several reported ultrafiltration devices.
- table S9. Yield and reliability analysis of CNT-STEM fabrication, assembly, and testing.
- note S1. Structure stiffness of N-MWCNT forest in the CNT-STEM.
- note S2. Device reliability study.
- References (*76*–*85*)

Other Supplementary Material for this manuscript includes the following:
(available at advances.sciencemag.org/cgi/content/full/2/10/e1601026/DC1)

- Data file S1 (Microsoft Excel format)

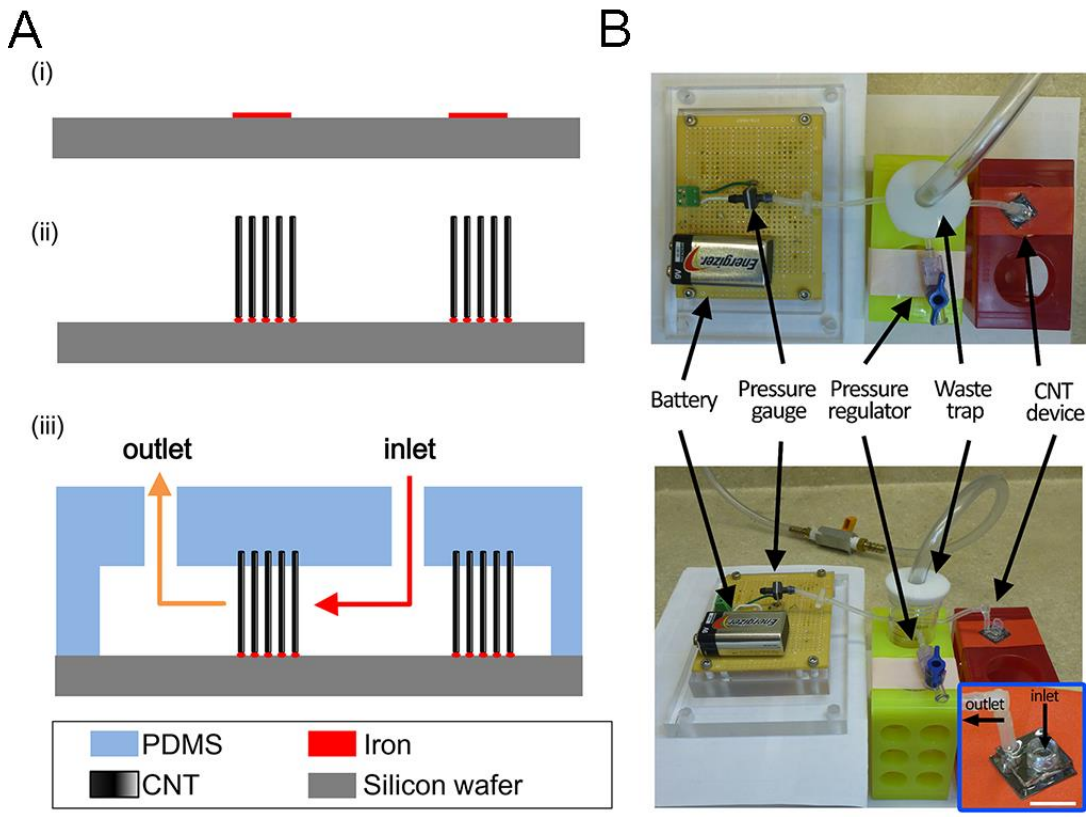

fig. S1. **Fabrication process and the testing setup of the CNT-STEM. (A)** Fabrication process of CNT-STEM. **(i)** Iron catalyst thin film was deposited on a prime silicon wafer and patterned by a lift-off process. **(ii)** The aligned CNT was selectively synthesized on patterned silicon surface during AACVD. **(iii)** CNT-STEM was formed by bonding a PDMS chamber with fluidic access to silicon substrate. Arrows label sample flow direction from the inlet to the outlet. **(B)** Top and side view of the testing setup. The virus-containing sample was first filtered through a membrane filter of 0.2 µm pore size (not shown here), then loaded into the sample reservoir at the inlet and processed through CNT-STEM via a vacuum source connected through a waste trap at the outlet. The vacuum pressure was measured by a miniature pressure sensor and regulated by a precision mechanical regulator. Inset shows the CNT-STEM device, scale bar: 1 cm.

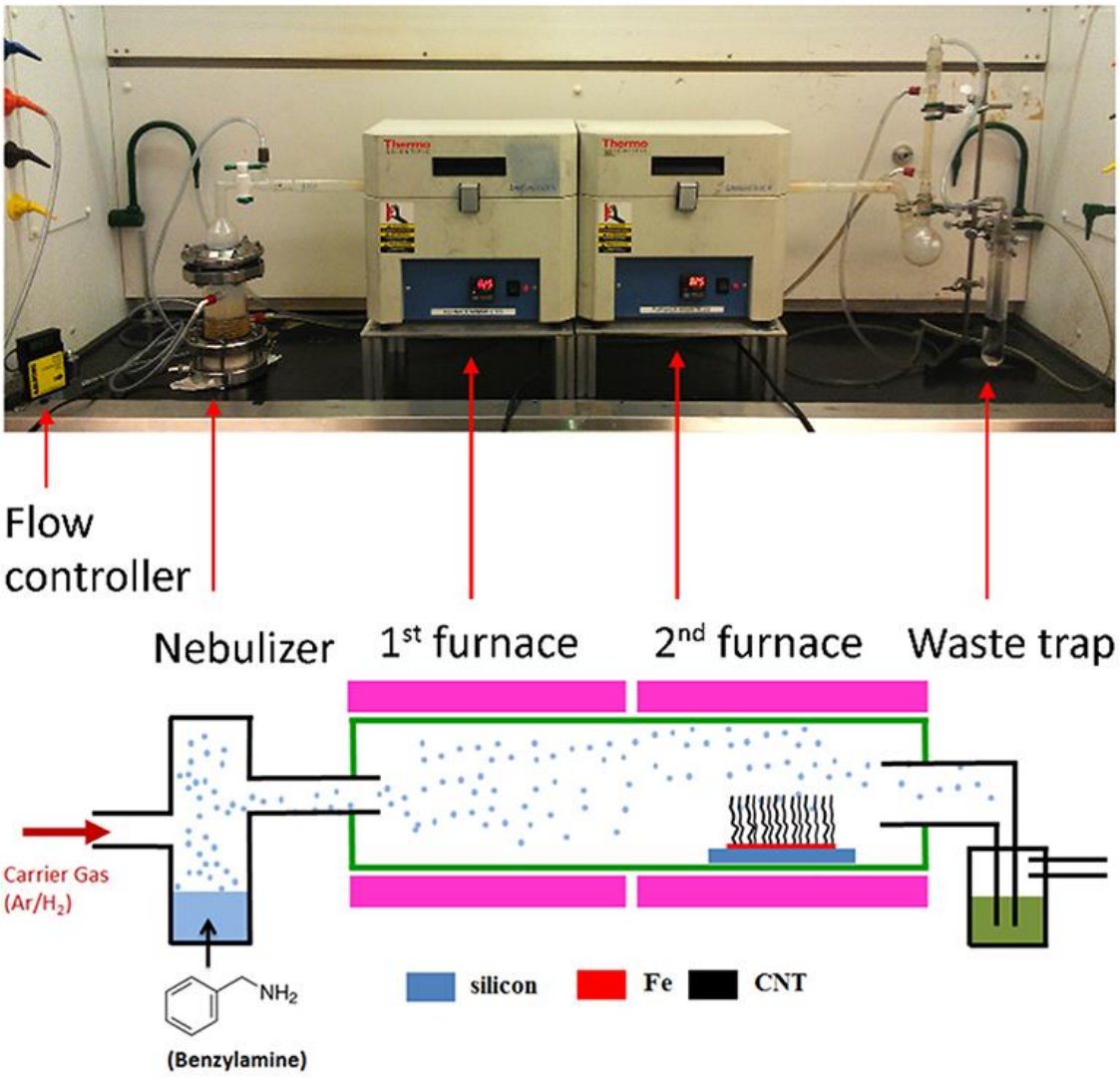

fig. S2. AACVD for N-MWCNT synthesis.

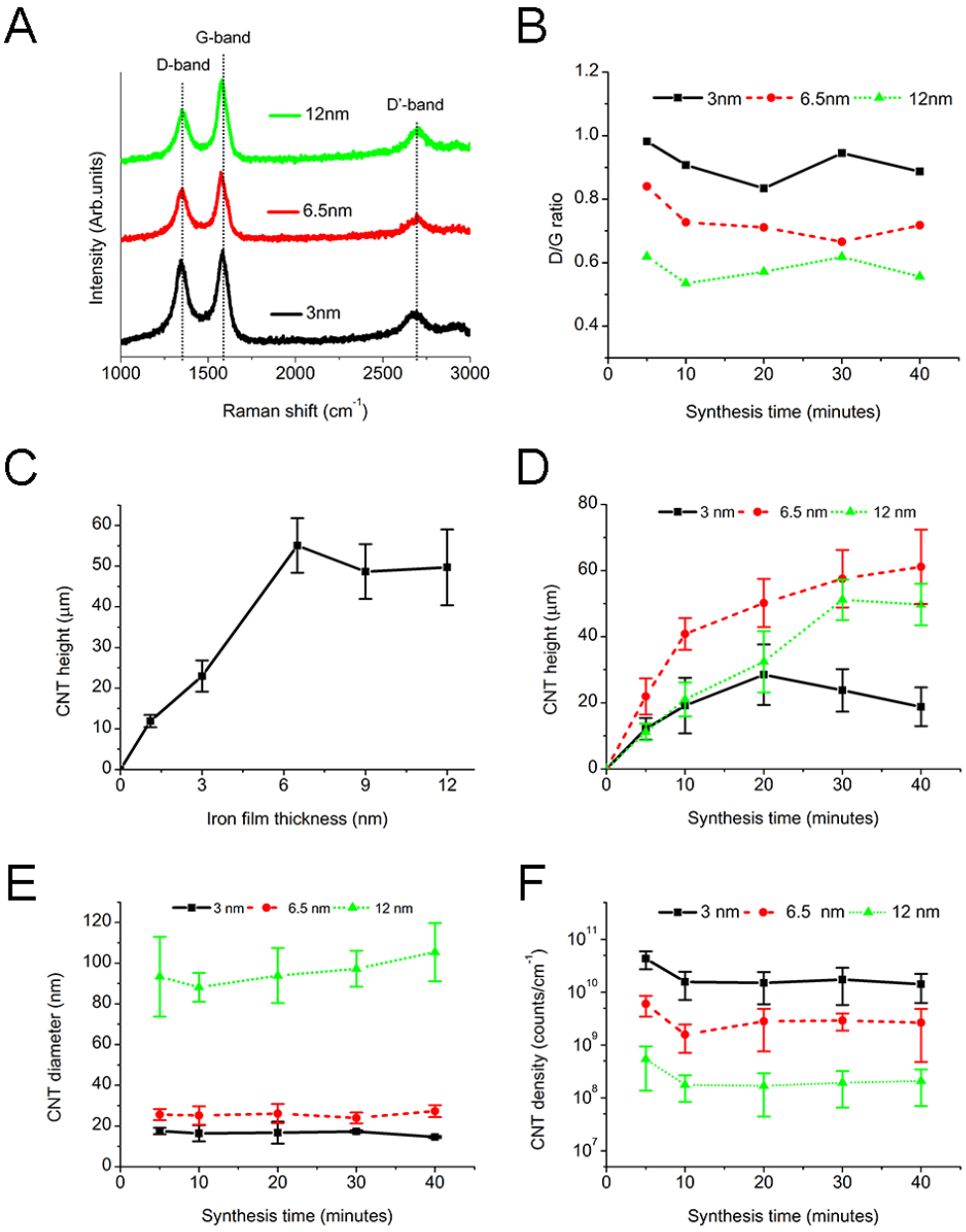

fig. S3. Raman spectra of the newly synthesized N-MWCNT structures on silicon substrates and the effect of the synthesis time on the height, diameter, and density of the aligned N-MWCNT structure. Geometrical parameters were measured from SEM images. **(A)** Raman spectra of the N-MWCNT structures synthesized on 3 nm, 6.5 nm and 12 nm thick iron catalyst thin films. The Raman spectra indicate the aligned N-MWCNT has D, G and D' band peaks at 1352, 1578 and 2659 cm^{-1}, respectively. The results are consistent with previous studies on N-MWCNT. **(B)** Plot of the peak height ratio of the D band and G band of the N-MWCNT structures formed on 3 nm, 6.5 nm and 12 nm thick iron catalyst thin films over synthesis time. Thicker iron catalyst layer results in lower D/G band ratio. **(C)** Height of N-MWCNT structure synthesized for 30 minutes on 1 nm, 3 nm, 6.5 nm, 9 nm and 12 nm thick iron thin films (n = 8). (b-d) The effect of the synthesis time on the height **(D)**, diameter **(E)** and linear density **(F)** of the N-MWCNT structure. The N-MWCNT was grown on 3 nm, 6.5 nm and 12 nm thick iron catalyst thin films under 5, 10, 20, 30 and 40 minutes of AACVD synthesis (n = 8).

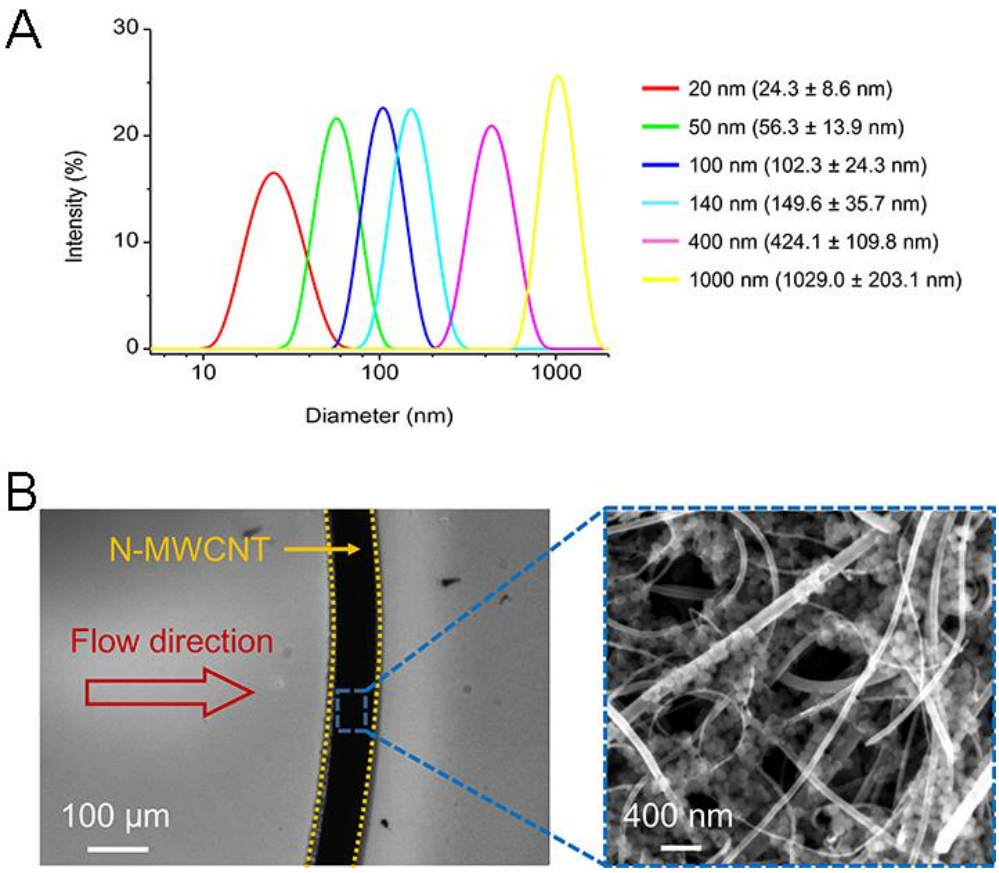

fig. S4. Characterization of size-based particle capture by CNT-STEM. (**A**) Diameter distribution of fluorescent polystyrene nanospheres measured by laser diffraction. (**B**) Florescence microscopic image showing the transport of 100 nm fluorescently labeled nanospheres in CNT-STEM device with 95 nm inter-tubular distance. Inset is a SEM image of nanospheres trapped inside N-MWCNT structure of the CNT-STEM.

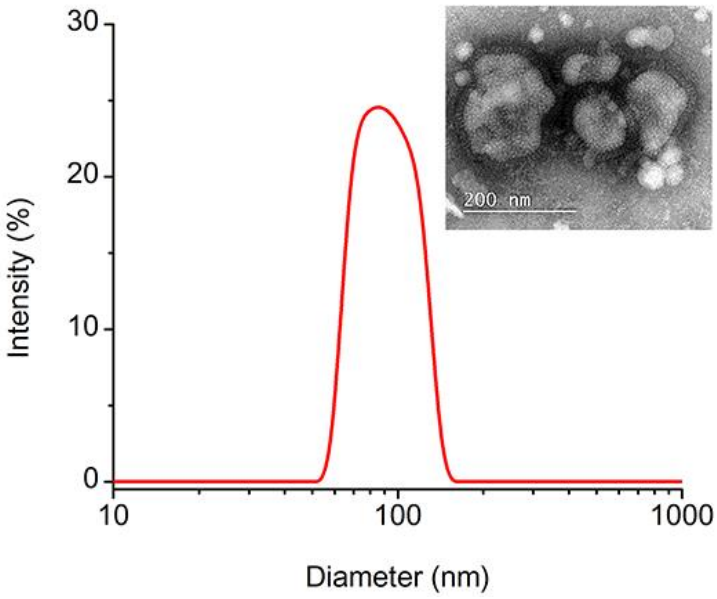

fig. S5. **Laser diffraction measurement of the size distribution of the LP AIV H5N2 strain used in this study.** Inset showed TEM image of the H5N2 virus. Scale bar, 200 nm.

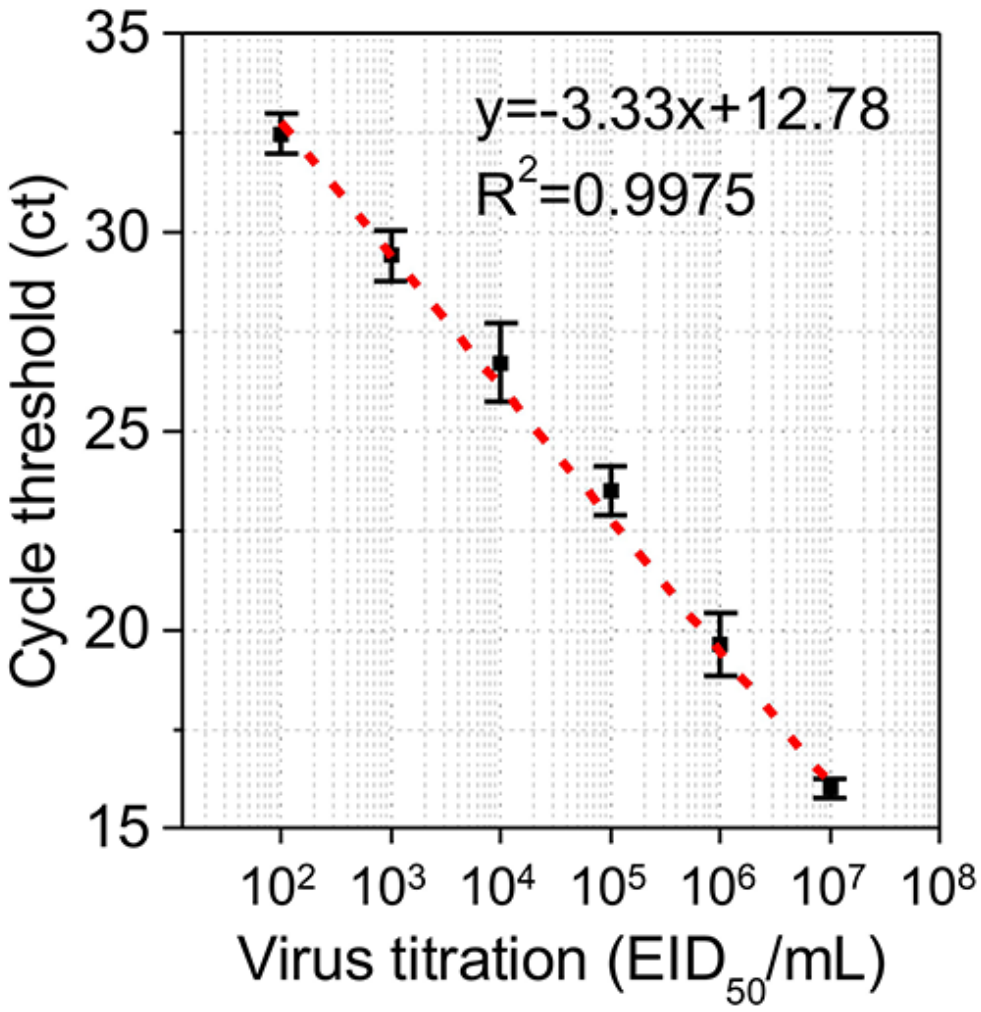

fig. S6. Standard curve for the rRT-PCR detection of H5N2 AIV (*n* = 4 each). The rRT-PCR assay had efficiency of 99.66% with the slope of the standard curve -3.33. The concentration of the original H5N2 sample (no dilution) was ~1.8×10^8 EID_{50}. No signal was detected after 10^7 dilution thus the detection limit here was 1.8×10^2 EID_{50}/mL.

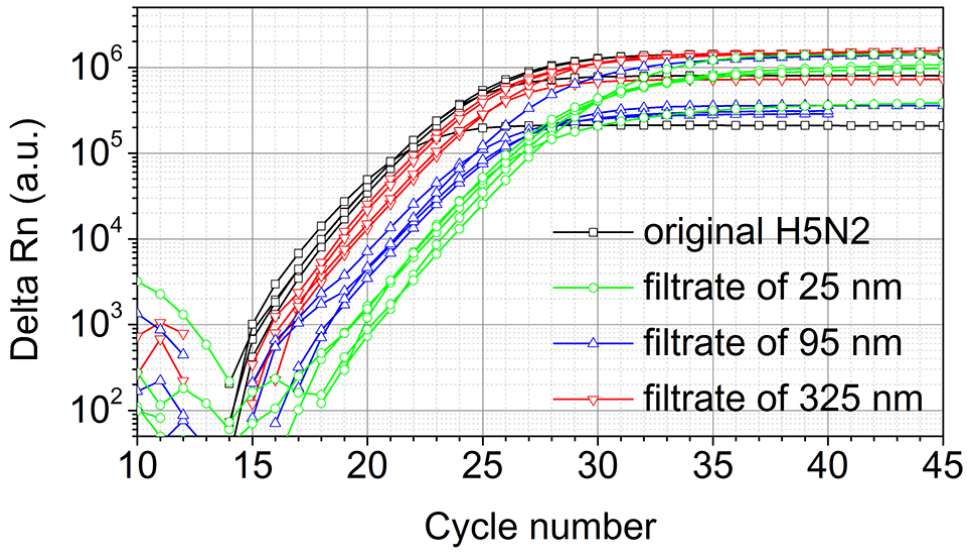

fig. S7. Capture efficiency measurement of CNT-STEM with 25-, 95-, and 325-nm intertubular distances when loading H5N2 AIV of 10^6 EID_{50}/ml titer into each device (*n* = 6). The Ct values of filtrates and the original sample were measured (*n* = 6 each).

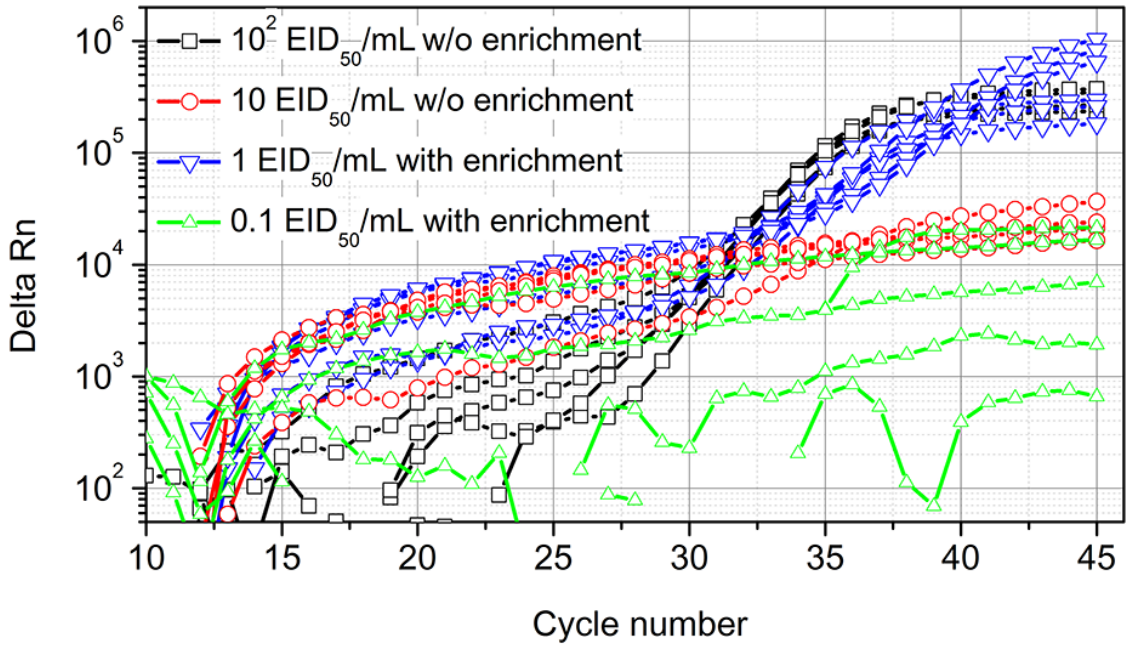

fig. S8. rRT-PCR curves of H5N2 AIV samples of 10 and 10^2 EID_{50}/ml titers without enrichment and those of 0.1 and 1 EID_{50}/ml titers with CNT-STEM enrichment (*n* = 6).

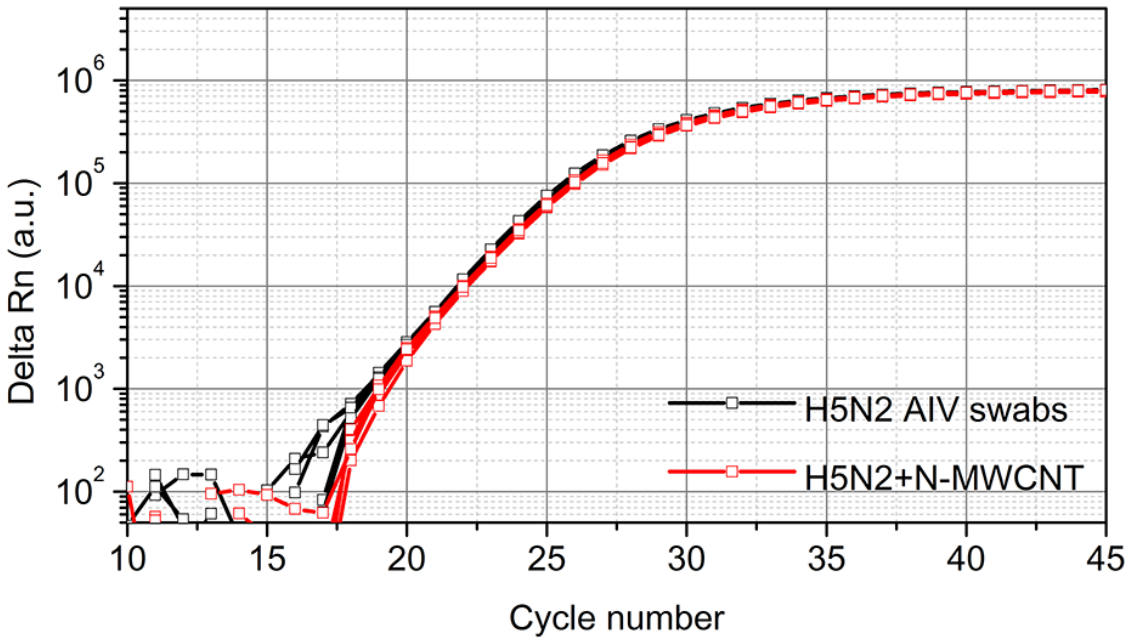

fig. S9. The compatibility test of N-MWCNT to rRT-PCR. The "H5N2 + N-MWCNT" samples were prepared by scraping N-MWCNT from the CNT-STEM without virus processing using razor blade and then mixed with swab-mimicking H5N2 AIV samples of 5×10^4 EID_{50}/ml titer for rRT-PCR detection (n = 5).

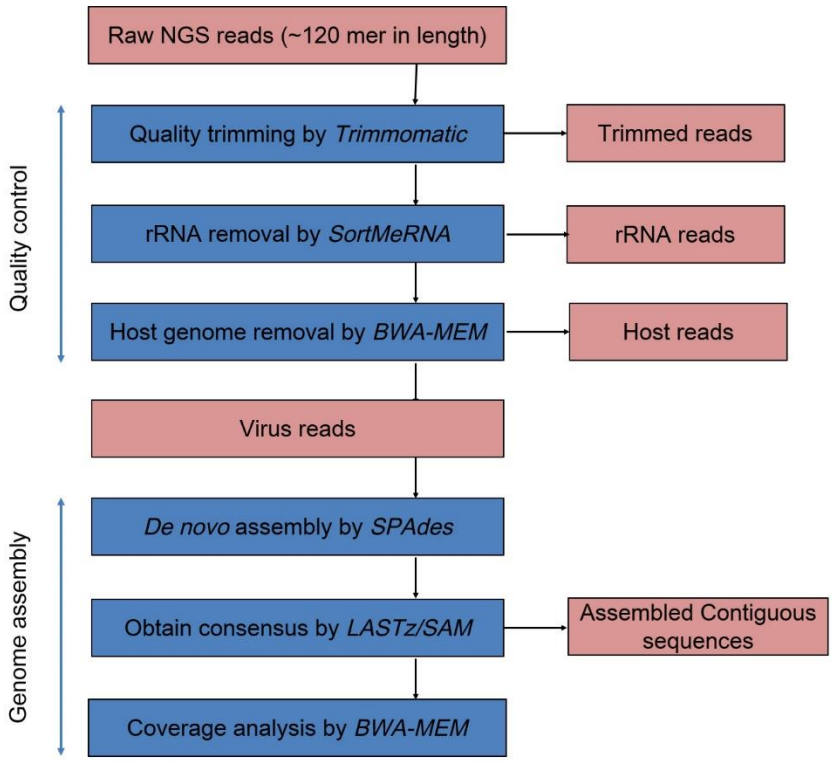

fig. S10. Diagram of data processing pipeline for NGS.

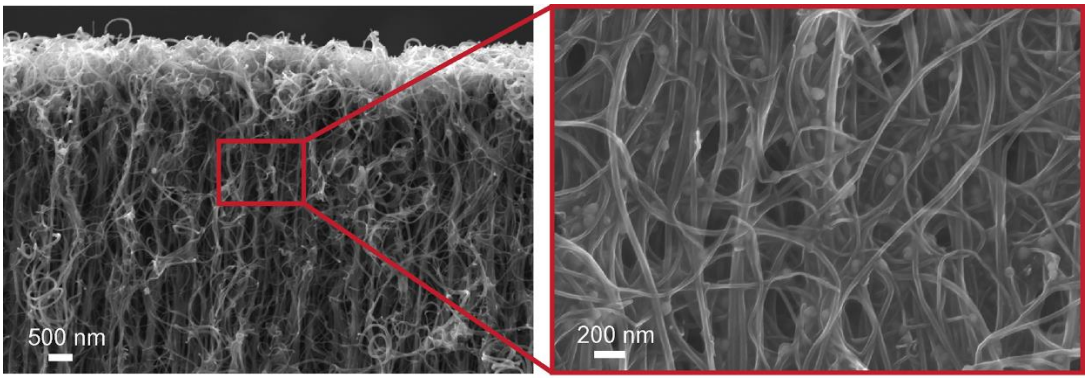

fig. S11. SEM images of CNT-STEM after processing field sample containing AIV.

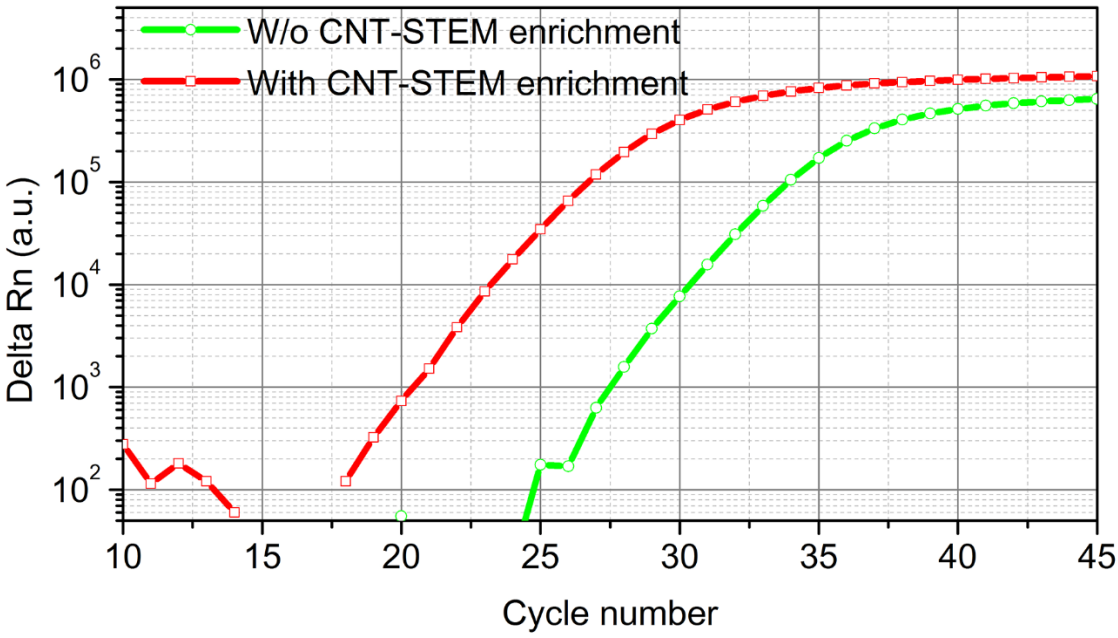

fig. S12. rRT-PCR detection of the H11N9 AIV duck swab with and without CNT-STEM enrichment.

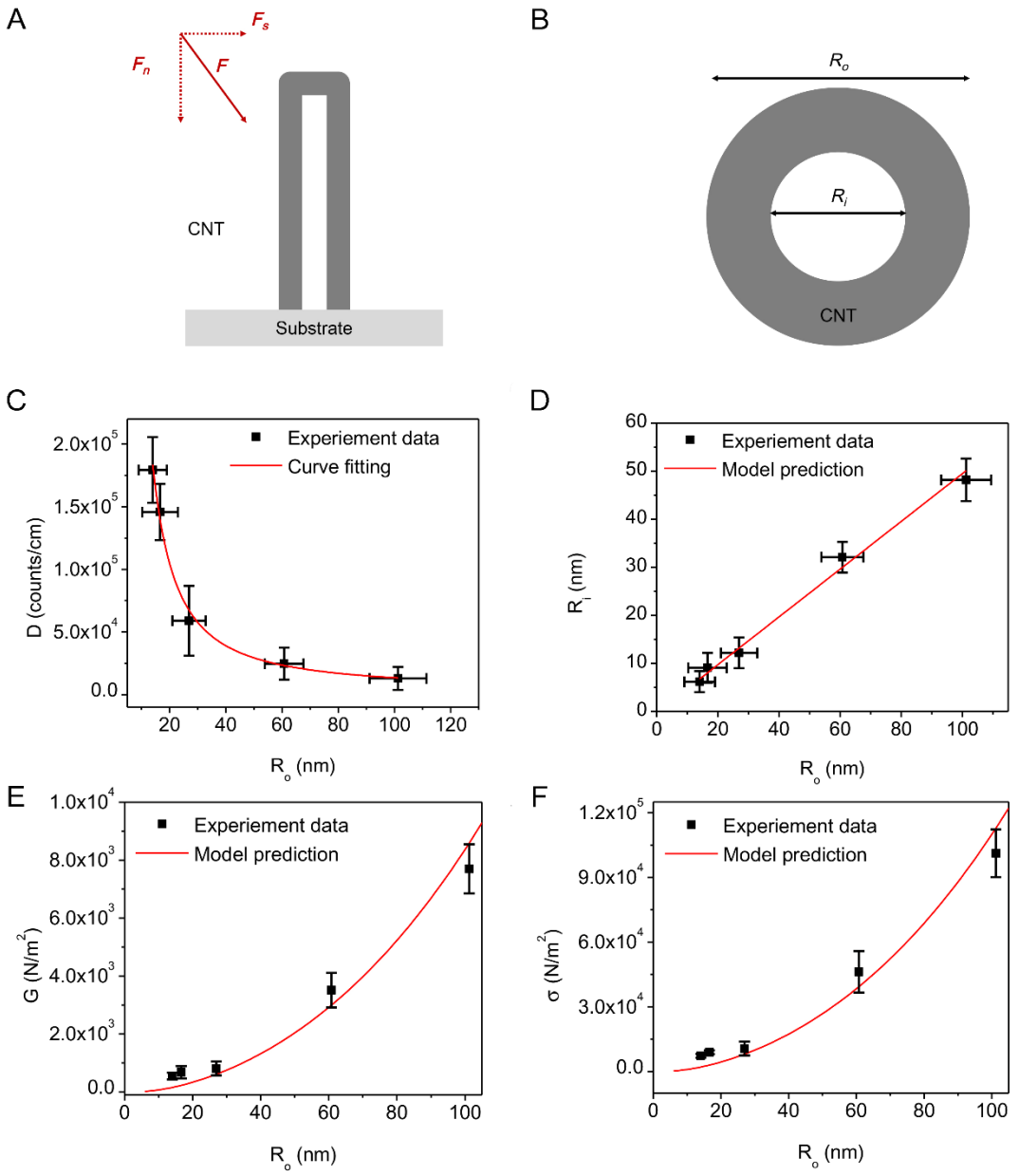

fig. S13. Structural mechanics analysis of N-MWCNT forest. (**A**) Illustration of a force (*F*) applied to hallow cylindrical N-MWCNT structure. *F* can be resolved into the shear force F_s and normal force F_n. (**B**) Geometry illustration of the outer diameter (R_o) and the inner diameter (R_i) of a N-MWCNT hallow cylindrical structure. (**C**) Plot of the measured linear density (***D***) versus outer diameter and the fitting curve. (**D**) Plot of measured inner diameter versus outer diameter and the fitted curve. (**E**) Plot of shear modulus (*G*) of the N-MWCNT forest versus fitted N-MWCNT outer diameter under a shear force loading. Calculated *G* based on measured N-MWCNT diameter is labeled as "Experimental data". (**F**) Plot of the critical buckling stress (σ) versus N-MWCNT outer diameter under a normal force loading.

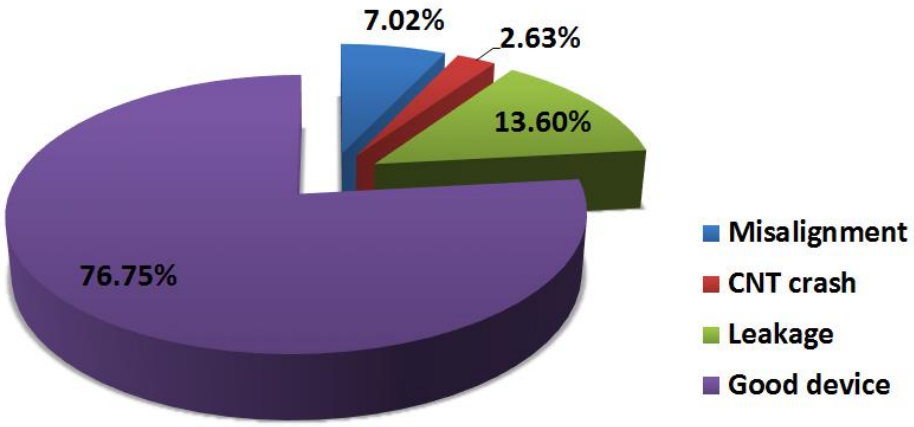

fig. S14. Analysis device yield, reliability, and failure modes. Good devices are CNT-STEMs that are successfully fabricated, assembled and tested. Failed devices can be cataloged as misalignment during device fabrication (Misalignment), mishandling resulted in N-MWCNT structure crash (CNT crash) and leakage during quality check of flow filtration (Leakage).

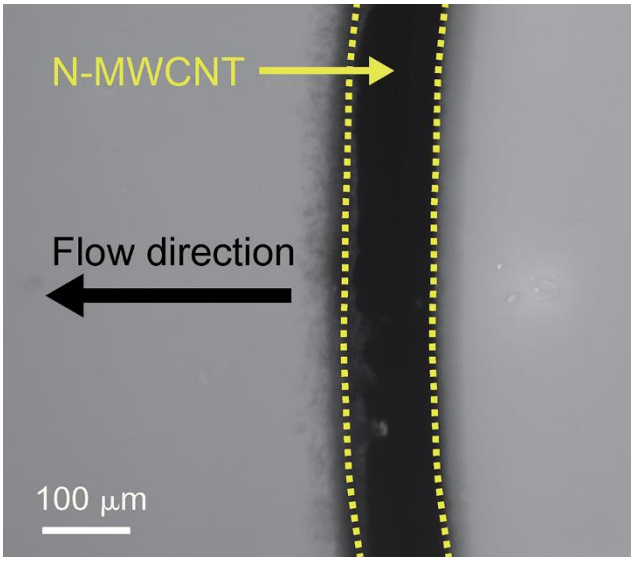

fig. S15. Fluorescent image of FITC-conjugated IgG pass through CNT-STEM of 25-nm in intertubular distance.

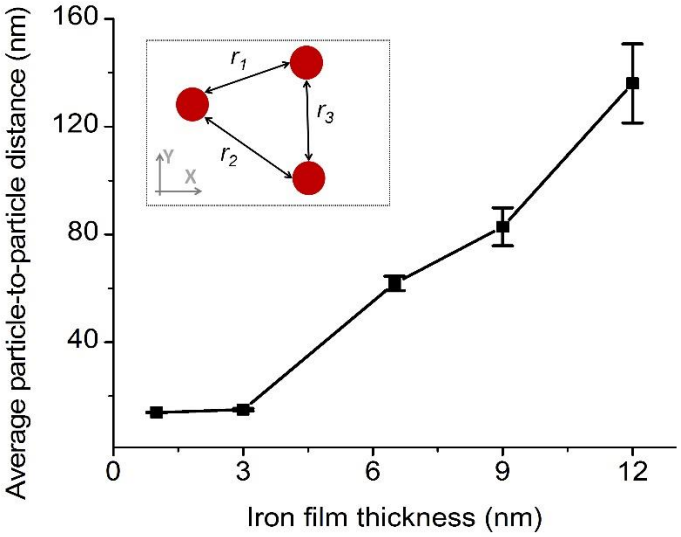

fig. S16 Calculated distance between the iron particles based on the Delaunay triangle selection algorithm. The inset illustrates the geometry definition of nearest neighbor particles. The average particle-to-particle distance is the mean of r_1, r_2 and r_3.

table S1. Measurement of the intertubular distance of N-MWCNT forest and the corresponding critical particle sizes of CNT-STEM.

Iron catalyst thickness (nm)	N-MWCNT		Critical particle sizes of CNT-STEM (nm)
	Inter-tubular distance (nm)	Standard deviation (nm)	
1	17	6	-
3	25	10	~35
6.5	95	25	~80
9	194	40	-
12	325	56	~225

table S2. Assembled contigs of the LP H5N2 AIV sample enriched by CNT-STEM.

Segment	Contig length (nt)	Ave. seq. depth (min/max)	Closest H5N2 strain in Genbank			
			Highest similarity strain (sequence ID)	Length (nt)	Identities	Gaps
PB2	2316	8446±4870 (3427/25340)	A/turkey/MN/3689-1551/1982(H5N2) (EU743285)	2315	99% (2315/2316)	0/2316
PB1	2316	10388±3464 (3376/22974)	A/turkey/MN/3689-1551/1982(H5N2) (EU743284)	2306	99% (2305/2306)	0/2306
PA	2259	12334±2268 (1935/18966)	A/mallard/New York/189/1982(H5N2) (CY014854)	2225	99% (2204/2225)	0/2225
HA	1742	12221±2751 (1820/18275)	A/mallard/WI/411/1981(H5N2) (CY179411)	1742	99% (1732/1742)	0/1742
NP	1633	13921±3190 (1453/21459)	A/turkey/MN/3689-1551/1982(H5N2) (EU743282)	1539	100% (1539/1539)	0/1539
NA	1452	12819±2835 (729/18292)	A/G-W teal/WI/432/1981(H5N2) (CY179405)	1442	99% (1437/1439)	0/1439
M1/M2	1047	15646±3986 (2241/28076)	A/turkey/MN/1598/1981(H5N2) (CY014761)	1015	99% (1013/1015)	0/1015
NS1/NS2	905	14804±4022 (1138/22400)	A/turkey/MN/3689-1551/1981(H5N2) (U85382)	865	100% (865/865)	0/865
Total	***13670***			***13450***		***0***

table S3. Phylogenetic analysis of the sequenced H5N2 strain (A/chicken/PA/7659/1985) to closely related H5N2 AIV strains isolated from United States/Canada in Genbank.

A) HA

		% Nucleotide identity																	
	Strain	1	2	3	4	5	6	7	8	9	10	11	12	13	14	15	16	17	18
% Amino acid identity	1	***	99.5	97.6	97.3	96.9	94.5	94.4	94.4	94.4	94.3	94.3	94.2	94.2	94.2	94.2	94.2	94.1	93.9
	2	99.3	***	97.8	97.7	97	94.5	94.4	94.5	94.3	94.4	94.4	94.4	94.2	94.3	94.2	94.3	94.3	94.1
	3	98.3	98.7	***	99.2	99.2	94.9	94.4	94.9	94.7	94.3	94.7	94.7	94.6	94.6	94.5	94.6	94.5	94.4
	4	97.9	98.5	99.6	***	98.5	94.7	94.3	94.7	94.5	94.3	94.5	94.5	94.3	94.4	94.3	94.4	94.3	94.2
	5	97.7	98.1	99.5	99.1	***	94.6	94	94.6	94.4	93.9	94.4	94.4	94.5	94.3	94.2	94.3	94.2	94.1
	6	98.1	98.3	98.8	98.4	98.3	***	95.3	99.9	99.7	95.4	99.2	99.2	98.5	99.1	95.3	99.1	98.7	98.8
	7	96.1	96.3	96.5	96.1	96	96.9	***	95.2	95	99.5	95.2	95.2	95.1	95.1	99.5	95.1	95	94.9
	8	97.9	98.3	98.8	98.4	98.3	99.7	96.7	***	99.7	95.4	99.2	99.2	98.5	99.1	95.2	99.1	98.7	98.8
	9	97.9	97.7	98.3	97.9	97.7	99.2	96.1	99.2	***	95.2	99	99	98.3	98.9	95	98.9	98.5	98.6
	10	96.3	96.4	96.7	96.3	96.1	97.1	99.3	96.8	96.3	***	95.4	95.4	95.3	95.3	99.3	95.2	95.1	95
	11	97.7	98.1	98.4	98	97.9	99.3	96.5	99.3	98.8	96.7	***	99.4	98.5	99.4	95.2	99.7	98.7	98.8
	12	97.5	97.9	98.1	97.7	97.6	99.1	96.5	99.1	98.5	96.7	98.9	***	98.4	99.3	95.2	99.3	98.6	98.7
	13	98	98.1	98.4	98	97.9	99.3	96.5	99.1	98.5	96.7	98.9	98.7	***	98.4	95.1	98.3	98.3	98.3
	14	97.6	98	98.3	97.9	97.7	99.2	96.4	99.2	98.7	96.5	99.1	98.8	98.8	***	95.1	99.2	98.6	98.7
	15	96.1	96.3	96.5	96.1	96	96.9	99.7	96.7	96.1	99.3	96.5	96.5	96.5	96.4	***	95	94.9	94.8
	16	97.6	98	98.3	97.9	97.7	99.2	96.4	99.2	98.7	96.5	99.3	98.8	98.8	98.9	96.4	***	98.5	98.6
	17	97.9	98.5	98.3	98.1	97.7	98.9	96.1	98.9	98.4	96.3	98.8	98.5	98.8	98.7	96.1	98.7	***	99.2
	18	97.7	98.1	98.4	98	97.9	99.1	96.3	99.1	98.5	96.4	98.9	98.7	98.9	98.8	96.3	98.8	99.1	***

Label	Strain (accession number)	Label	Strain (accession number)
1	A/chicken/PA/7659/1985(H5N2)(KP674444)	**11**	A/fowl/OR/459674-5/2006(H5N2)(GQ923133)
2	A/mallard/WI/411/1981(H5N2)(CY179403)	**12**	A/pintail/BC/07813/2005(H5N2)(CY095268)
3	A/mallard/AL/847/1975(H5N2)(CY179763)	**13**	A/mallard/MN/346250/2000(H5N2)(CY139689)
4	A/duck/AL/57/1976(H5N2)(CY005918)	**14**	A/mallard/BC/373/2005(H5N2)(DQ826532)
5	A/goose/WI/711/1975(H5N2)(EF607857)	**15**	A/rhea/TX/39923/1993(H5N2)(EU743106)
6	A/goose/AK//445210/2006(H5N2)(GU050182)	**16**	A/duck/OR/459674-3/2006(H5N2)(GU049986)
7	A/chicken/NJ/17169/1993(H5N2)(EU743019)	**17**	A/bird/WI/439436/2006(H5N2)(GU050174)
8	A/goose/AK/477003/2007(H5N2)(GQ923397)	**18**	A/teal/CA/HKWF609/2007(H5N2)(CY033444)
9	A/waterfowl/CO/443593/2006(H5N2)(GQ923517)		
10	A/chicken/PA/3609/1993(H5N2)(CY034681)		

B) NA

		% Nucleotide identity																
	Strain	1	2	3	4	5	6	7	8	9	10	11	12	13	14	15	16	17
% Amino acid identity	1	***	99.1	99	98.9	98.9	98.5	98.4	94.9	94.9	94.8	94.7	94.7	94.7	94.7	94.7	94.6	94.4
	2	99	***	99.3	99.1	99.1	97.7	97.5	94.2	94.1	94	93.9	93.8	94	94	93.9	94	93.7
	3	99.2	98.9	***	99.8	99.7	97.7	97.5	94.3	94.4	94.4	94	93.9	94.2	94.1	94.3	94.1	94.1
	4	99.2	98.9	99.7	***	99.8	97.6	97.4	94.2	94.4	94.4	93.9	93.8	94.2	94.1	94.3	94.1	94.1
	5	98.9	98.6	99.4	99.7	***	97.5	97.3	94.1	94.3	94.3	93.9	93.8	94.1	94.1	94.2	94	94
	6	98.9	97.9	98.1	98.1	97.8	***	99.7	94.5	94.5	94.3	94.3	94.1	94.1	94.3	94.3	94.3	94.3
	7	99	98.1	98.2	98.2	97.9	99.8	***	94.5	94.4	94.3	94.2	94.1	94.1	94.3	94.3	94.2	94.2
	8	97	96.3	96.2	96.2	95.8	96.5	96.6	***	98.3	97.4	99.1	95.5	97.2	97.6	97.4	97.6	97.2
	9	96.5	95.8	96	96	95.7	96.3	96.5	97.6	***	97.7	98.2	95.8	97.4	97.9	97.7	97.8	97.5
	10	97.4	96.8	96.6	96.6	96.3	97.3	97.4	98.6	98.4	***	97.6	95.5	99.5	98.6	99.7	98.6	99.4
	11	96.8	96.2	96	96	95.7	96.3	96.5	98.9	97.4	98.4	***	95.4	97.3	97.8	97.4	97.8	97.1
	12	96.8	96.2	96	96	95.7	96.6	96.8	97	96.8	97.8	96.8	***	95.2	95.2	95.4	95.2	95.2
	13	97.8	97.1	97	97	96.6	97	97.1	98.6	98.1	99.7	98.4	97.4	***	98.3	99.3	98.3	99
	14	97.4	96.8	96.6	96.6	96.3	97.3	97.4	98.6	98.4	99.7	98.4	97.8	99.4	***	98.6	99.8	98.3
	15	97.1	96.5	96.3	96.3	96	97	97.1	98.2	98.1	99.7	98.1	97.4	99.4	99.4	***	98.6	99.4
	16	97.4	96.8	96.6	96.6	96.3	97.3	97.4	98.6	98.4	99.7	98.4	97.8	99.4	100	99.4	***	98.3
	17	96.6	96	96.2	96.2	95.8	97.1	97.3	97.8	97.9	99.2	97.6	97	98.9	98.9	98.9	98.9	***

Label	Strain (accession number)	Label	Strain (accession number)
1	A/chicken/PA/7659/1985(H5N2)(KP674445)	**11**	A/chukkar/MN/14591-7/1998(H5N2)(AY300926
2	A/mallard/WI/411/1981(H5N2)(CY179405)	**12**	A/pheasant/NJ/1355/1998(H5N2)(AY300927)
3	A/mallard/WI/1616/1983(H5N2)(CY178112)	**13**	A/duck/IL/08OS2688/2008(H5N2)(CY079454)
4	A/widgeon/WI/493/1983(H5N2)(CY178088)	**14**	A/turkey/NY/465977/2006(H5N2)(GQ117163)
5	A/teal/WI/568/1983(H5N2)(CY178096)	**15**	A/duck/OH/470655/2007(H5N2)(GQ923543)
6	A/goose/WI/711/1975(H5N2)(FJ517332)	**16**	A/waterfowl/CO/476466-3/2007(H5N2)(GQ923
7	A/mallard/AL/847/1975(H5N2)(CY179765)	**17**	A/pintail/FL/480645-5/2007(H5N2)(GQ92340
8	A/environment/NY/5626-1/1998(H5N2)(EU742		
9	A/mallard/MD/790/2002(H5N2)(EU980481)		
10	A/duck/MN/462960-2/2006(H5N2)(GQ923175)		

table S4. Assembled contigs of the H11N9 AIV field sample enriched by CNT-STEM.

Segment	Contig length (nt)	Ave. seq. depth (min/max)	Closest H5N2 strain in Genbank			
			Highest similarity strain (sequence ID)	Length (nt)	Identities	Gaps
PB2	2324	13±2 (1/25)	A/blue-winged Teal/North Dakota/AI09-2912/2009(H6N1) (CY140760)	2307	99% (2303/2307)	0/2307
PB1	2316	12±4 (1/22)	A/blue-winged teal/New Brunswick/00288/2010(H5N2) (CY138318)	2316	99% (2311/2314)	0/2314
PA	2210	14±6 (1/18)	A/American black duck/New Brunswick/02629/2007(H3N8) (CY129051)	2201	99% (2201/2205)	0/2205
HA	1744	12±1 (2/18)	A/Anas acuta/New Mexico/A00629381/2008(H11N9) (KF542875)	1740	99% (1730/1740)	0/1740
NP	1592	11±1 (1/21)	A/mallard/Minnesota/AI06-962/2006(H4N8) (CY139972)	1541	99% (1522/1524)	0/1524
NA	1435	11±2 (2/18)	A/mallard/Iowa/3193/2009(H11N9) (CY097584)	1435	99% (1427/1435)	0/1435
M1/M2	1008	11±3 (1/28)	A/green winged teal/Delaware/468157-6/2006(H5N2) (GU050076)	1027	100% (1007/1007)	0/1007
NS1/NS2	862	14±4 (1/22)	A/northern pintail/Illinois/464067-4/2006(H5N9) (GU051984)(gb|U85382.1|)	865	99% (856/858)	0/858
Total	***13491***			***13432***		***0***

table S5. Phylogenetic analysis of the emerging H11N9 strain (A/duck/PA/02099/2012) to previously reported and closely related AIV strains.

A) HA

		% Nucleotide identity													
	Strain	1	2	3	4	5	6	7	8	9	10	11	12	13	14
% Amino acid identity	1	***	99.9	99.3	98.3	98.1	98.1	97.9	97.8	97.7	97.3	97.3	96.5	95.9	92.8
	2	99.7	***	99.2	98.1	97.9	98	97.7	97.7	97.6	97.2	97.3	96.4	95.8	92.7
	3	99.1	98.8	***	97.6	97.4	97.5	97.2	97.4	97	96.6	96.7	95.8	95.3	92.3
	4	99.7	99.5	98.8	***	99.4	96.9	96.6	96.6	96.4	96.6	97.5	96	95.3	92
	5	99.3	99.1	98.4	99.3	***	96.6	96.3	96.4	96.1	96.3	97.3	95.8	95.1	91.7
	6	98.8	98.5	97.9	98.8	98.4	***	99.1	96.3	98.9	95.9	95.8	95.1	94.3	91.5
	7	98.5	98.3	97.6	98.5	98.1	99.2	***	96.2	99	95.6	95.5	95	94.1	91.3
	8	98.4	98.1	98	98.3	97.7	97.7	97.5	***	95.9	96.1	95.9	95.3	94.8	91.4
	9	98.3	98	97.3	98.3	97.9	98.9	99.2	97.2	***	95.4	95.3	94.8	94	91.3
	10	98.1	97.9	97.2	98.1	97.7	97.7	97.5	96.8	97.2	***	96.1	98.5	97	93.5
	11	98.3	98.3	97.3	98.3	97.9	97.3	97.1	96.7	96.8	97.7	***	95.5	94.5	91.4
	12	97.7	97.5	96.8	97.7	97.5	97.6	97.9	96.7	97.1	98.3	97.3	***	96.6	92.8
	13	98.7	98.4	97.7	98.7	98.3	98	97.7	97.2	97.5	98.4	97.7	98	***	93.5
	14	97.1	96.8	96.7	97.1	96.7	96.4	96.2	95.9	95.9	97.3	96.8	96.7	97.3	***

Label	Strain (accession number)	Label	Strain (accession number)
1	A/duck/PA/2099/2012(H11N9)(KR870237)	**11**	A/mallard/MS/11OS5863/2011(H11N9)(CY166760)
2	A/mallard/MN/Sg-00118/2007(H11N9)(CY078050)	**12**	A/mallard/MN/346246/2000(H11N9)(DQ424860)
3	A/Anas_acuta/NM/A00629381/2008(H11N9)(KF542875)	**13**	A/mallard/MD/538/2002(H11N9)(GQ257487)
4	A/mallard/CA/6634/2008(H11N9)(CY094125)	**14**	A/mallard/WI/456/1984(H11N9)(CY021661)
5	A/mallard/CA/10125/2008(H11N9)(CY093671)		
6	A/shoveler/IL/10OS3619/2010(H11N9)(CY133029)		
7	A/mallard/WI/10OS4193/2010(H11N9)(CY133045)		
8	A/mallard/AK/44430-056/2008(H11N9)(HM193587)		
9	A/mallard/OH/12OS4697/2012(H11N9)(CY186822)		
10	A/mallard/MN/182722/1998(H11N9)(CY139745)		

B) **NA**

		% Nucleotide identity																	
	Strain	1	2	3	4	5	6	7	8	9	10	11	12	13	14	15	16	17	18
% Amino acid identity	1	***	99.8	99.5	99.5	99.4	99.4	99.3	99.2	98.7	98.7	98.4	98.3	98.3	98	97.7	97.5	97.4	97.2
	2	99.3	***	99.6	99.6	99.5	99.5	99.4	99.3	98.5	98.4	98.1	98.1	98.1	97.7	97.4	97.3	97.2	97
	3	98.4	98.7	***	100	99.3	99.7	99.6	99.5	98.2	98.1	97.8	97.8	97.8	97.4	97.1	97	96.9	96.9
	4	98.4	98.7	100	***	99.3	99.7	99.6	99.5	98.2	98.1	97.8	97.8	97.8	97.4	97.1	97	96.9	96.9
	5	98.6	98.9	98.9	98.9	***	99.3	99.2	99.1	98.1	98.1	97.8	97.7	97.7	97.4	97.2	96.9	96.8	96.7
	6	98.2	98.6	99.1	99.1	98.7	***	99.5	99.7	98.1	98.1	97.8	97.7	97.7	97.4	97.1	96.9	96.8	96.6
	7	98.2	98.6	99.1	99.1	98.7	98.9	***	99.3	98	98	97.7	97.7	97.6	97.4	97.1	96.9	96.8	96.6
	8	97.8	98.2	98.7	98.7	98.4	99.3	98.6	***	98	97.9	97.6	97.5	97.5	97.2	96.9	96.8	96.6	96.5
	9	96.6	95.8	94.9	94.9	95.1	94.8	94.8	94.4	***	97.4	97.1	97.1	97.1	99.1	98.7	98.4	98.3	98.4
	10	97.3	96.6	95.7	95.7	95.8	95.5	95.5	95.1	93.9	***	99.6	99.5	99.5	97	96.7	96.4	96.3	96.3
	11	96.2	95.5	94.6	94.6	94.8	94.4	94.4	94	92.8	98.9	***	99.9	99.6	96.7	96.4	96.1	96	96.1
	12	96	95.3	94.4	94.4	94.6	94.2	94.4	93.9	92.6	98.7	99.8	***	99.5	96.7	96.4	96.1	96	96.1
	13	96.2	95.5	94.6	94.6	94.8	94.4	94.4	94	92.8	98.9	98.9	98.7	***	96.6	96.3	96	95.9	96
	14	94.2	93.5	92.6	92.6	92.8	92.4	92.8	92.1	97.3	92.6	91.5	91.5	91.5	***	98.5	98.1	98	98.7
	15	93.7	93	92.4	92.4	92.6	92.2	92.6	91.9	96.4	92.1	91	91	91	95.8	***	98.1	98	97.8
	16	93.7	93	92.1	92.1	92.2	91.9	92.2	91.5	96	91.3	90.3	90.3	90.3	95.3	95.3	***	99.3	97.4
	17	93.5	92.8	91.9	91.9	92.1	91.7	92.1	91.3	95.8	91.2	90.1	90.1	90.1	94.9	95.1	98	***	97.3
	18	92.4	91.7	91.5	91.5	91.2	90.6	90.8	90.3	95.5	90.8	90.1	90.1	90.1	96.2	93.9	93.1	93.3	***

Label	Strain (accession number)	**Label**	Strain (accession number)
1	A/duck/PA/2099/2012(H11N9)(KR870239)	**11**	A/shorebird/DE/351/2009(H1N9)(CY137916)
2	A/mallard/MN/Sg-00118/2007(H11N9)(CY078052)	**12**	A/turnstone/NJ/AI09-1082/2009(H1N9)(CY146281)
3	A/goldeneye/IW/3192/2009(H11N9)(CY097068)	**13**	A/turnstone/Ilha_de_Canelas/A51/2008(H11N9)(KF824506)
4	A/mallard/IA/3193/2009(H11N9)(CY097584)	**14**	A/teal/OH/467/2001(H11N9)(GU053360))
5	A/mallard/OH/2033/2009(H4N9)(CY097119)	**15**	A/knot/DE/650666/2002(H11N9)(CY144334)
6	A/mallard/WI/4203/2009(H11N9)(CY097424)	**16**	A/pintail/AB/22/1997(H2N9)(CY116777)
7	A/mallard/AR/AI09-5663/2009(H11N9)(CY141011)	**17**	A/duck/WA/663/1997(H11N9)(EF599119)
8	A/teal/OH/12OS2138/2012(H10N9)(CY186865)	**18**	A/mallard/MD/439/2002(H11N9)(GQ257481)
9	A/mallard/AB/31/2001(H3N9)(CY004701)		
10	A/turnstone/NJ/Sg-00561/2008(H11N9)(CY145689)		

table S6. Comparison of contigs of the unknown virus (IBDV/Turkey/PA/00924/14) generated by de novo assembly after CNT-STEM enrichment and NGS to the closest IBDV strains in Genbank.

			Comparison to the closest IBDV strains in Genbank				
Segment	**Contig length (nt)**	**Average sequencing depth (min/max)**	**Highest similarity strain (sequence ID)**	**Length (nt)**	**Identities**	**Gaps**	**Host**
A	3258	806±255(219/1028)	Infectious bursal disease virus segment A (U30818)	3254	94% (3070/3259)	12/3259	Gallus
B	2857	1307±450 (377/2623)	Infectious bursal disease virus segment B (AY918949)	2827	95% (2698/2827)	0/2807	Edgar
Total	***6044***			***6013***		***11***	

table S7. Single-nucleotide polymorphism/variant analysis of the "unknown" virus (IBDV/turkey/PA/00924/14) to sequenced IDBV virus strains.

A) VP2, VP3, VP4

		% Nucleotide identity																
	Strain	1	2	3	4	5	6	7	8	9	10	11	12	13	14	15	16	17
% Amino acid identity	1	***	93.9	91.3	84	84	83.9	83.8	83.8	83.8	83.8	83.7	83.7	83.7	83.7	83.6	83.5	83.4
	2	97	***	91	83.7	83.8	83.7	83.7	83.6	83.5	83.6	83.5	83.5	83.5	83.5	83.5	83.3	83.3
	3	97.3	96.7	***	83.5	83.6	83.3	83.5	83.5	83.5	83.5	83.4	83.3	83.3	83.4	83.3	83.2	83.2
	4	91.4	90.3	91.6	***	99.8	99.7	98.1	98.1	98.1	98.1	98.1	98	99.1	98	98	97.7	97.7
	5	91.4	90.3	91.6	100	***	99.5	98.3	98.2	98.3	98.2	98.2	98.2	99.1	98.1	98.2	97.9	97.8
	6	91	90.2	91.3	99.6	99.6	***	97.8	97.8	97.8	97.8	97.8	97.8	98.9	97.7	97.8	97.5	97.4
	7	91.3	90.4	91.5	98.8	98.8	98.4	***	99.8	99.7	99.9	99.7	99.7	98.2	99.7	99.7	99.5	99.4
	8	91.2	90.3	91.4	98.8	98.8	98.4	99.8	***	99.7	99.8	99.7	99.7	98.2	99.8	99.7	99.6	99.5
	9	91.2	90.1	91.4	98.8	98.8	98.4	99.4	99.4	***	99.7	99.8	99.9	98.1	99.6	99.9	99.4	99.3
	10	91.1	90.2	91.3	98.6	98.6	98.2	99.8	99.6	99.2	***	99.7	99.8	98.2	99.7	99.8	99.4	99.4
	11	91.1	90	91.3	98.9	98.9	98.5	99.5	99.5	99.7	99.3	***	99.8	98.1	99.6	99.8	99.3	99.3
	12	90.9	90	91.1	98.7	98.7	98.3	99.5	99.5	99.7	99.5	99.6	***	98.1	99.6	99.9	99.3	99.3
	13	91.1	90	91.4	99.2	99.2	98.8	99	99	98.8	98.8	98.9	98.7	***	98.1	98.1	97.8	97.8
	14	90.9	90	91.1	98.5	98.5	98.1	99.5	99.7	99.1	99.3	99.2	99.2	98.7	***	99.6	99.8	99.7
	15	90.9	90	91.1	98.7	98.7	98.3	99.5	99.5	99.7	99.5	99.6	100	98.7	99.2	***	99.3	99.3
	16	90.4	89.5	90.6	98	98	97.6	99	99.2	98.6	98.8	98.7	98.7	98.2	99.5	98.7	***	99.5
	17	90.4	89.5	90.6	97.9	97.9	97.5	98.9	99.1	98.5	98.7	98.6	98.6	98.1	99.4	98.6	98.9	***

Label	Strain (accession number)	**Label**	Strain (accession number)
1	00924(2014)(KP642112)	**11**	CS-2-35(2008)(EF418033)
2	OH(2007)(U30818)	**12**	CT(2001)(AJ310185)
3	23/82(2001)(AF362773)	**13**	IM(2004)(AY029166)
4	A-BH83(2011)(JF811920)	**14**	JD1(2002)(AF321055)
5	HPR-2(2008)(EF418036)	**15**	Gt(2007)(DQ403248)
6	STC(2007)(D00499)	**16**	HZ2(2002)(AF321054)
7	903/78(2012)(JQ411012)	**17**	ZJ2000(2002)(AF321056)
8	D78(2004)(AF499929)		
9	H-30(2008)(EF418035)		
10	P2(2003)(X84034)		

B) VP1

		% Nucleotide identity															
	Strain	1	2	3	4	5	6	7	8	9	10	11	12	13	14	15	16
% Amino acid identity	1	***	95.4	95.3	95.2	95	95	94.9	94.7	93.4	93.1	91.3	90.5	90.5	90.2	90.1	89.5
	2	95.4	***	99.6	95.7	98.3	98.2	98.6	95.1	95.9	95.8	92.4	90.2	90.3	90.1	89.6	89.6
	3	95.3	99.6	***	95.6	98.1	98.1	98.5	95	95.8	95.8	92.2	90.1	90.3	90.1	89.6	89.5
	4	95.2	95.7	95.6	***	95.3	95.3	95.4	95.3	93.7	93.8	91.5	90.9	90.8	90.6	90.1	90
	5	95	98.3	98.1	95.3	***	100	98.3	94.7	95.4	95.7	92.9	90.1	90	89.7	89.4	89.2
	6	95	98.2	98.1	95.3	100	***	98.3	94.6	95.4	95.6	92.9	90.1	89.9	89.7	89.3	89.2
	7	94.9	98.6	98.5	95.4	98.3	98.3	***	94.8	95.8	96.7	92.5	90.3	90.2	89.9	89.6	89.6
	8	94.7	95.1	95	95.3	94.7	94.6	94.8	***	93.1	92.8	90.7	90.3	91.1	90.9	90.5	89.5
	9	93.4	95.9	95.8	93.7	95.4	95.4	95.8	93.1	***	93.6	90.9	89.6	89.5	89.4	88.7	88.6
	10	93.1	95.8	95.8	93.8	95.7	95.6	96.7	92.8	93.6	***	90.5	89.7	89.4	89.4	88.7	89.1
	11	91.3	92.4	92.2	91.5	92.9	92.9	92.5	90.7	90.9	90.5	***	89.5	88.3	88.1	88	88.1
	12	90.5	90.2	90.1	90.9	90.1	90.1	90.3	90.3	89.6	89.7	89.5	***	93.1	93	92.5	92.6
	13	90.5	90.3	90.3	90.8	90	89.9	90.2	91.1	89.5	89.4	88.3	93.1	***	99.3	97.2	91.7
	14	90.2	90.1	90.1	90.6	89.7	89.7	89.9	90.9	89.4	89.4	88.1	93	99.3	***	96.9	91.5
	15	90.1	89.6	89.6	90.1	89.4	89.3	89.6	90.5	88.7	88.7	88	92.5	97.2	96.9	***	91.2
	16	89.5	89.6	89.5	90	89.2	89.2	89.6	89.5	88.6	89.1	88.1	92.6	91.7	91.5	91.2	***

Label	Strain (accession number)	Label	Strain (accession number)
1	00924(2012)(KP642112)	**11**	HN04(2013)(KC109815)
2	Edgar(2007)(AY918949)	**12**	HLJ-7(GQ452269)
3	Lukert(2007)(AY918947)	**13**	SK53(2014)(KJ198845)
4	23/82(2001)(AF362774)	**14**	HLJ-4(2010)(GQ449689)
5	GA-1(2008)(EU162094)	**15**	ZZ-11(2012)(JX682712)
6	ViBursa(2008)(EU162092)	**16**	QL(2012)(JX682710)
7	A-BH83(2011)(JF811921)		
8	OH(2007)(U30819)		
9	MG1(2013)(JN982246)		
10	GX-NNZ-11(2012)(JX134484)		

table S8. Comparison of CNT-STEM to several reported ultrafiltration devices.

Ultrafiltration Devices	Pore size (nm)	Thickness	Operating pressure (kPa)	Flux (m/s)[a]	Normalized resistance (/m)[b]	Permeability (m^2)[c]	Porosity	Tunable range (nm)	Reference
Hydrophilized PVDF (Millipore Viresolve 180)	12-18	150 μm	103	$1.4\text{-}1.5\times10^{-4}$	$6.9\text{-}7.4\times10^{11}$	2.1×10^{-16}	-	-	(*76, 77*)
Hydrophilized PVDF (Pall DV20)	20	40 μm	155	2.1×10^{-7}	7.5×10^{14}	5.4×10^{-20}	-	20, 50	(*76*)
Nanoporous block co-polymer	15	80 nm	10	$1.1\text{-}1.4\times10^{-5}$	$7.2\text{-}9.0\times10^{11}$	1.0×10^{-19}	20%	10-40	(*78*)
Anodized aluminum oxide membrane	16	-	98	1.3×10^{-6}	7.5×10^{13}	-	-	15-401	(*79-83*)
	20	60 μm	150	4.4×10^{-4}	3.4×10^{11}	1.8×10^{-16}	25-50%		
Track etched polycarbonate (Nuclepore)	15	6.5 μm	10	$0.8\text{-}1.1\times10^{-7}$	$0.9\text{-}1.2\times10^{14}$	6.1×10^{-20}	2%	15-8,000	(*78*)
			196	1.8×10^{-6}					(*83*)
CNT-STEM	**25**	**100 μm**	**0.69**	$\mathbf{1.2\times10^{-4}}$	$\mathbf{5.9\times10^{9}}$	$\mathbf{1.7\times10^{-14}}$	**78%**	**17-325**	**This study**
	95			$\mathbf{7.7\times10^{-4}}$	$\mathbf{9.0\times10^{8}}$	$\mathbf{1.1\times10^{-13}}$	**92%**		

a: Flux (m/s) J_v is either taken directly from references or calculated by using volumetric flow rate Q and cross-sectional area A as $J_v = \frac{Q}{A}$

b: Normalized resistance R_m is calculated from flux J_v, viscosity μ, and operation pressure ΔP using $R_m = \frac{-\Delta P}{\mu J_v}$ (*84*)

c: Permeability κ can be calculated from normalized resistance R_m and membrane thickness using $k = \frac{L}{R_m}$

table S9. Yield and reliability analysis of CNT-STEM fabrication, assembly, and testing.

	Steps	Yield	Failure mode	Counts (failure)
Fabrication	Iron patterning/dicing	100% (228/228)		0
	N-MWCNT synthesis	100% (228/228)		0
	PDMS bonding	93% (212/228)	Misalignment	16
	Assembly	97.2% (206/212)	CNT crash by mishandling	6
Testing	Device quality check	85.1% (175/206)	Leakage	31
	Virus filtration	100% (175/175)		0
	RNA extraction	100% (175/175)		0
Total		76.8% (175/228)		53

note S1. Structure stiffness of N-MWCNT forest in the CNT-STEM.

The structure stiffness of the N-MWCNT forest is important for the construction and successful operation of the CNT-STEM. The N-MWCNT forest is higher than the chamber depth of the PDMS chamber. The sealing between the N-MWCNT forest and the PDMS chamber is through the compressive force of the N-MWCNT forest without any adhesive in between. CNT has the largest elastic (Young's) modulus among all the materials. We studied the effect of N-MWCNT diameter on the aggregated structure stiffness of the N-MWCNT structure.

When force is applied to a single vertical N-MWCNT, we consider the N-MWCNT is a straight hollow cylinder and the force is resolved into two components: F_s is the shear force perpendicular to the N-MWCNT axial direction, and F_n is the normal force along the axial direction of the N-MWCNT (fig. S13A). We considered the effects of shear force and normal force separately.

A small deflection *d* of a hollow cylinder caused by an applied shear load can be described as following (*85*)

$$d = \frac{F_s L^3}{3EI} \qquad \text{(Equation S1)}$$

$$I = \frac{\pi}{4}\left(R_o^4 - R_i^4\right) \qquad \text{(Equation S2)}$$

where *L* is the length of the cylinder, *E* is the elastic modulus of the cylinder material, *I* is the moment of inertia of the cylinder, R_o and R_i are the outer and inner radii of the cylinder (fig. S13B).

We applied this equation to the structural stability of CNT-STEM by considering the shear stress τ that the N-MWCNT forest can withstand, which is determined by the shear force to a single N-MWCNT F_s and its linear density (λ, N-MWCNT counts per unit length) of the N-MWCNT forest

$$t = F_s \lambda^2 \qquad \text{(Equation S3)}$$

From Equations S1-S3, the shear modulus G, can be defined as

$$G = \frac{t}{d/L} = \frac{3p}{4}\frac{E\left(R_o^4 - R_i^4\right)I^2}{L^2} \quad \text{(Equation S4)}$$

We measured the N-MWCNT linear density λ and the inner diameter R_i. Both can be fitted into expressions using the N-MWCNT outer diameter R_o in polynomial forms (fig. S13C&D)

$$I = 2.2 \times 10^3 + 8.9 \times 10^5 R_o^{-1} + 2.3 \times 10^7 R_o^{-2} \ \text{(counts/cm)}, \ R^2 = 0.993 \quad \text{(Equation S5)}$$

$$R_i = 0.50 R_o - 0.20 \ \text{(nm)}, \ R^2 = 0.989 \quad \text{(Equation S6)}$$

Assuming E = 500 GPa (*38*) , L = 40 µm, the shear modulus of the N-MWCNT structure is a function of N-MWCNT outer diameter

$$G = 3.3 \times 10^{-5} R_o^4 + 2.7 \times 10^{-2} R_o^3 + 6.2 R_o^2 + 2.9 \times 10^2 R_o + 3.7 \times 10^3 + 3.8 \times 10^2 R_o^{-1} - 2.3 \times 10^2 R_o^{-2} + 62 R_o^{-3} - 6.2 R_o^{-4} \quad \text{(Pa, } R_o \text{ in nm)} \quad \text{(Equation S7)}$$

We plotted this equation based on measured N-MWCNT diameter data and the fitting equation (fig. S13E). It is clear that large outer diameter improves the overall structure stiffness. For the CNT-STEM, it means the N-MWCNT forest can withstand larger shear stress if N-MWCNTs of larger diameter are used.

Based on the fundamental mode of buckling to a column fixed on both ends, the critical axial bucking force F_n exceeding which the structure is under unstable equilibrium can be calculated as (*85*)

$$F_n = \frac{4p^2 EI}{L^2} \quad \text{(Equation S8)}$$

Thus the critical buckling stress (force per area) σ is

$$s = F_n D^2 = \frac{4p^2 EID^2}{L^2} = \frac{p^3 E\left(R_o^4 - R_i^4\right)D^2}{L^2} \quad \text{(Equation S9)}$$

σ can be expressed as a function of the N-MWCNT outer diameter R_o

$$s = 4.5 \times 10^{-4} R_o^4 + 0.36 R_o^3 + 82 R_o^2 + 3.8 \times 10^3 R_o + 4.9 \times 10^4 + 5.0 \times 10^3 R_o^{-1} - 3.1 \times 10^3 R_o^{-2} + 8.3 \times 10^2 R_o^{-3} - 83 R_o^{-4} \quad \text{(Pa, } R_o \text{ in nm)} \quad \text{(Equation S10)}$$

We plotted this equation based on measurement data and the fitting equation (fig. S13F). Similarly to the case of the shear modulus, the larger the N-MWCNT diameter (R_o) has larger critical buckling stress (σ). This result suggests a N-MWCNT forest with a larger average diameter can withstand larger loading force to prevent buckling associated instability.

note S2. Device reliability study.

In table S9, we recorded and analyzed the device yield and reliability during the CNT-STEM fabrication, assembly and testing. The overall success rate from device fabrication to testing is 76.8% out of 228 fabricated devices. During device fabrication, the PDMS top chamber was aligned to the N-MWCNT forest patterns by naked eyes before bonding, 16 out of 228 devices (7.0%) failed because of the misalignment. Although the N-MWCNT forest structure can withstand pressure and forces during normal device operation, when it hits a hard surface during fabrication, it can still “crash”. This kind of mishandling accounts for 2.6% of overall device failure. Finally prior to virus filtration, we measured the flow rate during the PBS wash. We found 31 out of 206 devices has a leakage problem, which presented 58.5% (31/53) of all failure devices. We think the leakage was caused by some micro-scale damages of N-MWCNT structures, which compromised the integrity of the N-MWCNT porous wall and too miniscule to be observed under an optical microscope directly. To improve the yield of the device, some custom-made jigs or tools can be designed for automatic handling during the device fabrication, assembly and testing.